Lipid hydrogen isotope compositions primarily reflect growth water in the model archaeon *Sulfolobus acidocaldarius*

Carolynn M. Harris[a#], Sebastian Kopf[b], Jeemin H. Rhim[a,c], Alec Cobban[a], Felix J. Elling[d,e], Xiahong Feng[a], Jamie McFarlin[b,f], Yuki Weber[,d^], Yujiao Zhang[a%], Alice Zhou[a&], Harpreet Batther[b], Ann Pearson[d], William D. Leavitt [a,g]

[a] Department of Earth Sciences, Dartmouth College

[b] Department of Geological Sciences, University of Colorado at Boulder

[c] Department of Ecology, Evolution, and Marine Biology, U.C. Santa Barbara

[d] Department of Earth & Planetary Sciences, Harvard University

[e] Leibniz-Laboratory for Radiometric Dating and Isotope Research, Kiel University

[f] Department of Geology and Geophysics, University of Wyoming

[g] Department of Chemistry, Dartmouth College

Running head: Lipid hydrogen isotopes of S. acidocaldarius

Address correspondence to Carolynn M. Harris, carolynn.m.harris.gr@dartmouth.edu

[&] Current address: Connecticut Agricultural Experiment Station, New Haven, CT

[^] Current address: Chroma Medicine, Boston, MA

[%] Current address: National Center for Science & Technology Evaluation, P.R. China

Abstract

The stable hydrogen isotope composition (δ^2H) of lipid biomarkers can track environmental processes and remain stable over geologically relevant time scales, enabling studies of past climate, hydrology, and ecology. Most research has focused on lipids from the domain Eukarya (e.g., plant waxes, long-chain alkanes), and the potential of prokaryotic lipid biomarkers from the domain Archaea to offer unique insights into environments not captured by eukaryotic lipids remains unclear. Here, we investigate the H-isotope composition of biphytanes in *Sulfolobus acidocaldarius*, a model thermoacidophile and obligate heterotroph. We conducted a series of experiments that varied temperature, pH, shaking rate, electron acceptor availability, or electron donor flux. From these experiments, we quantified the lipid/water H-isotope fractionation ($^2\varepsilon_{L/W}$) values for core biphytane chains derived from tetraether lipids. The $^2\varepsilon_{L/W}$ values are consistently negative (-230 to -180 ‰) and are relatively invariant across all experiments despite a 20-fold change in doubling times and 2-fold change in lipid cyclization. The magnitude and relative invariance of $^2\varepsilon_{L/W}$ values are consistent with studies on other heterotrophic archaea and suggests archaeal lipids may be faithful recorders of the δ^2H composition of growth water. Our study highlights the potential of archaeal lipid $^2\varepsilon_{L/W}$ as a hydrological proxy, offering new insights into environments where traditional proxies, such as plant-derived lipids, are not available, including extreme environments and extraterrestrial settings.

Importance

Reconstructing past climates is crucial for understanding Earth's environmental history and its responses to changing conditions. This study examines *Sulfolobus acidocaldarius*, a thermoacidophilic archaeon that thrives in extreme environments like hot springs. These microorganisms incorporate hydrogen water in the growth environment into membrane lipids, creating hydrogen isotope signatures that can reflect hydroclimate conditions. Our findings show that these hydrogen isotope ratios remain consistent even under varying temperature, pH, oxygen levels, and electron donor fluxes, indicating a stable fractionation between lipids and water. This invariance suggests that *S. acidocaldarius* lipids could serve as a robust proxy for reconstructing ancient water H-isotope values, especially in extreme environments where traditional proxies, such as plant waxes, are absent. This research has broader implications for planetary-scale reconstructions, including potential applications in studying past climates on other planets, such as Mars, where similar microorganisms may have existed in hydrothermal conditions.

1. Introduction

The relative abundances of hydrogen isotopes ($^2H/^1H$) in water are set by physical, hydrological, and climatic factors (Gat 1996; Hayes 2001). Certain biomolecules incorporate these isotopes with a consistent offset (fractionation) relative to water, preserving a record of the isotopic composition (δ^2H values) of the water present during growth (Sessions et al. 1999). Some lipids can retain their original H-isotope composition for up to 10^8 years and lipid hydrogen isotope compositions have been used to study hydrologic and environmental change over millennia to millions of years, dating as far back as the Paleoproterozoic (Sessions et al. 2004; Dawson et al. 2004; Love and Zumberge 2021). Most studies of biomarker H-isotope composition focus on lipids from photoautotrophic organisms (e.g., plant wax *n*-alkanes) or chemoautotrophic and heterotrophic bacteria (e.g., fatty acids) (Sessions et al. 1999; Liu and An 2019; McFarlin et al. 2019; Ladd et al. 2021) and the H-isotope compositions recorded in lipids from the Archaea are comparatively poorly understood. A small, but growing, body of literature, however, has begun to address this gap (Kaneko et al. 2011; Dirghangi and Pagani 2013; Lengger et al. 2020; Wu et al. 2020; Leavitt et al. 2023; Rhim et al. 2024). Understanding the extent to which the δ^2H value of archaeal lipids records the δ^2H value of growth water requires a deeper examination of how environmental conditions impact this signal. A comprehensive investigation of the physicochemical factors affecting H-isotope fractionation between archaeal lipids and water ($^2\varepsilon_{L/W}$) is essential for employing archaeal lipid δ^2H composition as a proxy for the δ^2H composition of environmental water over space and time.

The $^2\varepsilon_{L/W}$ value for a biomolecule integrates both the composition of source water and the net biosynthetic fractionations resulting from the specific pathways used during lipid biosynthesis. Reported $^2\varepsilon_{L/W}$ values vary widely among domains of life. In phototrophic Eukaryotes (e.g., plants and algae), $^2\varepsilon_{L/W}$ values of waxes (e.g., n-alkanes) are consistently negative, ranging from -150 to -50 ‰ (Sachs 2014; McFarlin et al. 2019). It is important to understand the causes of this variability when applying lipid δ^2H values to reconstruct water δ^2H values. Net biosynthetic fractionation is generally consistent across taxa, though genetic factors introduce some variance (Gao et al. 2014; Bender et al. 2016; Baan et al. 2023; Baan 2024; Ladd et al. 2024; Pilecky et al. 2024). Environmental factors such as temperature, salinity, light availability, and CO_2 concentration, also influence $^2\varepsilon_{L/W}$ values, possibly via their impact on growth and biosynthesis rates (Sachs 2014; Sachs and Kawka 2015; Van Der Meer et al. 2015; Sachs et al. 2016; Maloney et al. 2016; Wolfshorndl et al. 2019; Torres-Romero et al. 2024). These effects are well-characterized in plants, and to a lesser extent in algae, and can be accounted for when the δ^2H values of plant waxes are used to reconstruct past hydroclimate (Sachse et al. 2012; Sessions 2016; McFarlin et al. 2019).

In contrast to the coherent magnitude and direction of $^2\varepsilon_{L/W}$ values observed from phototrophic eukaryotes, the $^2\varepsilon_{L/W}$ of bacterial fatty acids varies widely in both direction and magnitude (-400 ‰ to +300 ‰) (Sessions et al. 2002; Valentine 2009; Zhang et al. 2009a; Dawson et al. 2015; Leavitt 2016; Osburn et al. 2016; Leavitt et al. 2017; Wijker et al. 2019). Bacteria that use different central

energy metabolisms (e.g., chemoautotrophy, photoautotrophy, or heterotrophy) exhibit distinct ranges of $^{2}\varepsilon_{L/W}$ values, which has been attributed to differences in metabolic pathways and the substrate used for growth (e.g., simple sugars vs. tricarboxylic acid (TCA) cycle intermediates). A recent study suggests that variations in $^{2}\varepsilon_{L/W}$ values from aerobic heterotrophic bacteria are explained by energy fluxes through the intracellular hydride carriers $NADP^{+}$ and NADPH (Wijker et al. 2019). Given this metabolism-dependent heterogeneity, the $\delta^{2}H$ values of bacterial lipids in sediment records may have more utility as proxies for the energetic state of past microbial metabolisms (Zhang et al. 2009a; Osburn et al. 2016; Wijker et al. 2019).

Lipid-water ^{2}H-fractionation from the domain Archaea have been understudied to-date. From what we do know, $^{2}\varepsilon_{L/W}$ values have been reported for diether lipids (archaeol) in a mesophilic halophile (Dirghangi and Pagani 2013) and a methanogen (Wu et al. 2020), tetraether-derived biphytanes in three thermoacidophiles and one thermomesophile (Kaneko et al. 2011; Rhim et al. 2024), and one aerobic marine chemoautotroph (Leavitt et al. 2023), and whole tetraethers or tetraether-derived biphytanes in several environmental sediment samples (Kaneko et al. 2011; Lengger et al. 2020). The observed $^{2}\varepsilon_{L/W}$ values for these archaeal lipids are uniformly negative (i.e. -300 to -150 ‰) and similar in magnitude to those reported for isoprenoid lipids produced by eukaryotic phototrophs (e.g. C_{15} and C_{30} isoprenoids; Sessions et al. 1999; Sachs et al. 2016).

Our understanding of the factors controlling the H-isotope compositions of archaeal lipids are less developed than for the Eukarya and Bacteria. Recent experiments demonstrate that $^{2}\varepsilon_{L/W}$ is nearly constant over a range of growth rates in a marine autotroph (*Nitrosopumilus maritimus*; Leavitt et al., 2023) and that the impacts of carbon metabolism and growth phase on $^{2}\varepsilon_{L/W}$ are minor (*Archaeoglobus fulgidus*; Rhim et al., 2024). This relative invariance in $^{2}\varepsilon_{L/W}$ values is perhaps surprising considering the taxonomic and metabolic diversity of the investigated Archaea. The impact of environmental factors on this fractionation, however, has only been investigated within a single archaeal strain (*Haloarcula marismortui*; Dirghangi and Pagani 2013). Further investigation of the effects of multiple environmental factors on $^{2}\varepsilon_{L/W}$ in Archaea is crucial, particularly since many archaea are adapted to extreme environments that can experience both rapid and large changes to physicochemical conditions (Van de Vossenberg et al. 1998).

Isoprenoid glycerol dibiphytanyl glycerol tetraethers (iGDGTs) are archaeal lipids with particular relevance to paleoenvironmental reconstructions (Schouten et al. 2013). These tetraethers are structurally diagnostic, diagenetically robust, and routinely analyzed for paleoclimate reconstruction based on the relative abundances of specific structural moieties (Schouten et al. 2002, 2013; Pearson and Ingalls 2013). Archaea can synthesize a unique series of iGDGTs that contain from zero to eight cyclopentane rings (e.g., iGDGT-0 through iGDGT-8), though the most highly ringed moieties (iGDGT-7 and -8) have only been recovered from hydrothermal spring environments (De Rosa and Gambacorta 1988). Members of the Thaumarchaeota phyla can also produce crenarchaeol, an iGDGT containing four cyclopentane rings and one cyclohexyl ring (De

Rosa and Gambacorta 1988). The distribution of these moieties in natural systems is related to growth temperature and other environmental factors (Elling et al. 2014, 2017; Hurley et al. 2016; Cobban et al. 2020; Zhou et al. 2020) and forms the basis of the TEX_{86} paleo sea surface temperature proxy (Schouten et al. 2002). At low pH and high temperatures, Archaea synthesize more highly-ringed moieties as an adaptation to maintain membrane rigidity and reduce permeability. In hydrothermal systems, the ring distributions of thermoacidophilic archaea record the interactions between temperature, pH, energy availability, and other factors that influence growth rate (Zhou et al. 2020; Quehenberger et al. 2020; Yang et al. 2023).

To better understand the signals recorded by archaeal lipid δ^2H composition in natural systems, it is necessary to determine the extent to which environmental conditions influence $^2\varepsilon_{L/W}$ values. In this study, we determined the H-isotope fractionation between iGDGT-derived biphytanes and growth water ($^2\varepsilon_{L/W}$) for the thermoacidophilic and heterotrophic archaeon, *Sulfolobus acidocaldarius* (DSM 639). *S. acidocaldarius* evolved to grow optimally under multiple extreme conditions, namely low pH's, high temperatures, and low oxygen partial pressure (Brock et al. 1972; Bischof et al. 2019). For this work *S. acidocaldarius* was selected as a model organism because it thrives in extreme environments devoid of traditional eukaryotic lipid proxies (e.g., plant waxes), and because it can grow under a wide range of physicochemical conditions, with rapid doubling times and high biomass yields (Quehenberger et al. 2017).

Here we cultivated *S. acidocaldarius* over a range of physicochemical conditions that included shifts in temperature, pH, shaking rate, electron acceptor or electron donor flux. Changes in these environmental conditions are known to impact the growth rate and degree of iGDGT cyclization (Boyd et al., 2011; Jensen et al., 2015; Zhou et al., 2019; Quehenberger et al., 2020; Cobban et al., 2020), but their impact on lipid/water fractionation is unexplored. Understanding how these environmental factors influence lipid/water fractionation is critical for interpreting archaeal lipid δ^2H signatures in natural systems and refining their use as robust proxies for reconstructing past hydroclimate conditions.

2. Methods

2.1 Culture strains and growth

Axenic cultures of *S. acidocaldarius* (DSM 639) were grown aerobically under different environmental conditions (**Table 1**). Culture media was prepared following the Brock recipe in Wagner et al. (2012) with the following modifications (see *Substrate* column in Table 1). For all experiments, media contained 5.9 mmol L^{-1} (0.2% w/v) sucrose as the organic substrate. The electron donor flux experiments were also supplemented with 4.0 mmol L^{-1} (0.1% w/v) NZ-amine in addition to sucrose.

163 Growth was monitored photometrically at regular intervals throughout each experiment by
164 measuring the optical density (i.e., absorbance at 1 cm pathlength) of a culture aliquot at 600 nm
165 (OD_{600}) on a spectrophotometer. All experiments were inoculated to an initial OD_{600} between 0.004
166 and 0.008, using cells derived from an active pre-culture (grown on the same medium) in mid-
167 exponential phase. Specific growth rates (division day^{-1}; μ) were calculated using OD_{600}
168 measurements during the early to mid exponential phase after Cobban et al., (2020). Doubling time
169 (T_D) was calculated as:

170 **Eq. (1)** $$T_D\ (hours) = ln(2)/\mu$$

171 **2.2 Experimental conditions experiments**

172 We examined how temperature, pH, shaking rate, O_2 availability, and electron donor (sucrose) flux
173 influence H-isotope fractionation in *S. acidocaldarius* through a series of batch, fed-batch, and
174 chemostat experiments.

175 **Batch experiments:** Three sub-experiments were performed in which one environmental condition
176 (temperature, pH, or shaking rate) was systematically varied while holding the other two conditions
177 constant (previously described in Cobban et al., 2020). The reference conditions were 70 °C, pH 3,
178 and 200 RPM shaking rate. Shaking rate is considered a proxy for aeration rate, where faster speeds
179 increase oxygen availability in the media, though it also increases physical agitation.

180 Batch experiments were performed in temperature-controlled, shaking incubators (Innova-42,
181 Eppendorf) in 250 mL Erlenmeyer flasks containing 125 mL media covered with loose plastic caps to
182 reduce evaporation. Evaporation was further reduced by maintaining a 2L tray of water in the
183 incubator to humidify the atmosphere. All experiments were performed in quintuplicate. Biomass
184 samples were collected in mid-exponential phase by centrifuging (3214 x *g*; Eppendorf 5810 R, S-4-
185 104 rotor) 50 mL of culture for 15 minutes at 4 °C, the resulting cell pellets were stored at -80 °C until
186 lipid extraction.

187 **Fed-batch bioreactor experiments:** To more precisely determine the impact of oxygen availability,
188 we performed gas-fed batch experiments in bioreactors (previously described in Cobban et al.,
189 2020). Briefly, *S. acidocaldarius* was grown in 300 mL of medium in 1 L glass vessels. To modulate
190 availability (as flux) of the terminal electron acceptor O_2 was introduced to bioreactors at four
191 different partial pressures: 0.2, 0.5, 2.0 or 20 % (balance N_2). The O_2 dry mixing ratios 0.2, 0.5, and
192 2% were generated by mixing pure N_2 mixed with 2% O_2 at 9:1, 3:1, and 0:1 ratios, respectively, which
193 was controlled via my-Control PID controllers (Applikon, Delft, Netherlands). The 20% experiment
194 used a separate gas feedstock of Ultra ZeroGrade Air (AirGas). Culture conditions were maintained
195 at 70 °C, pH 3, stirred at 200 RPM (Rushton-type impeller), and at a total gas flux of 200 mL min^{-1}.
196 Each experiment was performed in triplicate via three bioreactors operated in parallel. Biomass

samples were collected by removing culture directly from the vessel, centrifuged at 4 °C, to pellet biomass, and then stored at -80 °C until lipid extraction.

Chemostat experiments: To determine the impact of electron donor flux, we performed chemostat experiments in which the dilution rate of the growth vessel was set to yield cell doubling times (T_D) of 7.0, 21.3, and 40.0 hours (previously described in Zhou et al. 2020). Briefly, *S. acidocaldarius* was grown in 300 mL of medium maintained at 70 ºC, pH 2.25, stirred at 200 RPM (Rushton-type impeller), and aerated with a constant flux of 200 mL min^{-1} Zero Air (ultra-high purity, UHP, AirGas/ AirLiquide, Inc.). Three chemostats were operated in parallel under continuous culture conditions. When steady state was achieved (assessed via regular OD_{600} measurements), biomass samples were harvested by continually collecting the outflow of each bioreactor into a chilled vessel (0 to 4 °C) for between 1 and 4 days, followed by centrifugation at 4 °C and storage at -80 °C prior to lipid processing. Multiple extracts representing 2 to 3 sampling events at identical growth rates were combined before lipid extraction.

2.3 Lipid extraction and derivatization

Core lipid fractions (iGDGTs) were extracted from lyophilized cell pellets via acidic hydrolysis-methanolysis (Elling et al. 2017; Zhou et al. 2020). iGDGTs were chemically derivatized to biphytanes to permit the determination of the δ^2H value of component biphytanes as described in Kaneko et al., (2011) and Leavitt et al., (2023). In brief, ether bonds were cleaved via digestion in 57% hydroiodic acid (HI) at 125 °C for 4 hours. The resulting alkyl iodides were hydrogenated (e.g., reduced to biphytanes, BPs) in H_2/PtO_2. An isotope dilution occurs when H is added during hydrogenation, which is corrected for during data processing and reduction (see Section 2.5).

2.4 Lipid identities & distributions

Isoprenoid BP chains were analyzed via GC-MS (Thermo ISQ LT with TRACE 1310) for compound identification and via GC-flame ionization detector (GC-FID; Thermo TRACE 1310) for compound quantification at the University of Colorado at Boulder Earth Systems Stable Isotope Lab (CUBES-SIL, Boulder, CO) (**FIG 1**). Biphytane yields and recovery were calculated using GC peak areas and co-injected n-alkane mixture as a quantification standard.

To describe the average amount of cyclopentyl rings in each BP distribution, we calculated a BP-Ring Index based on the relative abundance of each BP moiety (**Eq. 2**). This metric is similar to the iGDGT-based Ring Index (**Eq. 3**), which describes the average amount of cyclopentyl rings in a distribution based on the relative abundance of each iGDGT moiety (Zhang et al. 2016; Zhou et al. 2020).

Eq. (2)

$$RI_{BP} = \frac{BP{-}1 + (2 \cdot BP{-}2) + (3 \cdot BP{-}3)}{\sum_o^3 BP}$$

Eq. (3)

$$RI_{GDGT} = \frac{iGDGT{-}1 + (2 \cdot iGDGT{-}2) + (3 \cdot iGDGT{-}3) + \ldots + (8 \cdot iGDGT{-}8)}{\sum_o^8 iGDGT}$$

2.5 δ^2H analysis of media waters, substrates, and biphytane lipids

2.5.1 Media waters

Water samples for hydrogen isotope (δ^2H) analysis were collected concurrently with harvesting biomass for lipid analyses. Aliquots of filter-sterilized growth medium water was measured for δ^2H at the Stable Isotope Laboratory at Dartmouth College via a dual inlet isotope ratio mass spectrometer (IRMS; Thermo Delta Plus 304 XL) coupled to an H-Device (pyrolyzed to H_2 gas) for water reduction by chromium powder at 850°C (previously described in Kopec et al. (2018). The δ^2H_{Water} values were corrected using three laboratory standards spanning -161 to -7 ‰ vs. VSMOW, which were run every 8-10 samples. Analytical precision was <0.5 ‰.

2.5.2 Substrates

The δ^2H composition of non-exchangeable C-bound H from substrates used in growth media was analyzed in triplicate as trifluoroacetate derivatives via a Thermo Delta Plus XP coupled to a TC-EA (Abrahim et al. 2020). The δ^2H composition of sucrose was -93.0 ± 1.2 ‰.

2.5.3 Biphytanes

For all experiments, we report $^2\varepsilon_{L/W}$ values for biphytane (BP) hydrocarbons derived via ether cleavage from acid extractable iGDGTs. The δ^2H composition of individual BPs was determined by gas chromatography pyrolysis isotope ratio mass spectrometry (GC-P-IRMS) on a GC IsoLink II IRMS System (Thermo Scientific) at the University of Colorado at Boulder Earth Systems Stable Isotope Lab (CUBES-SIL, Boulder, CO). The system comprised a Trace 1310 GC fitted with a programmable temperature vaporization (PTV) injector and either a 30 m ZB5HT column (i.d. = 0.25 mm, 0.25 µm, Phenomenex, Torrance, CA, USA) or a 60 m DB1 column (i.d. = 0.25 mm, 0.25 µm, Agilent, Santa Clara, CA, USA), ConFlo IV interface, and 253 Plus mass spectrometer (Thermo Scientific).

2.5.4 Data reduction and notation

The δ^2H values of individual biphytanes (δ^2H_{BP}) were measured relative to H_2 reference gas (δ^2H_{raw}) and calibrated to the international references scale (VSMOW) using a standard n-alkane mixture (A7, containing C15 through C30 n-alkanes spanning -9 to -263 ‰ vs. VSMOW; A. Schimmelmann,

Indiana University). The A7 standard was combined with a C_{36} n-alkane (nC_{36}, -259.2 ‰ vs. VSMOW; A. Schimmelmann, Indiana University) and measured throughout each analytical run at regular intervals and at different concentrations. The BP hydrogen isotope calibration was performed as in Leavitt et al., (2023) using the R packages *isoreader* (v 1.3.0) and *isoprocessor* (v 0.6.11) available at github.com/isoverse (Kopf et al. 2021). In brief, δ^2H_{raw} values were corrected for offset, scale compression and peak-size effects using an inverted multivariate linear regression which was applied to all standards and samples to determine δ^2H_{cal} values. Further details of calibration and data reduction are available in Leavitt et al., 2023. The total analytical uncertainty of the corrected δ^2H_{BP} values was calculated using standard error propagation of the peak-size adjusted error estimates and hydrogenation correction assuming all errors to be uncorrelated. The hydrogenation correction ranged from 10.3 to 12.7 ‰ and increased analytical uncertainty by up to 1.9 ‰.

All $^2H/^1H$ ratios are reported in delta notation (δ^2H) in permil (‰) units relative to the international seawater standard on the VSMOW-SLAP (Vienna Standard Mean Ocean Water, Standard Light Antarctic Precipitation) scale.

Eq. (4)

$$\delta^2H\ (‰) = \left(\frac{^2H/\ ^1H_{Sample}}{^2H/\ ^1H_{Standard}} - 1\right)$$

All fractionation factors are reported in epsilon notation ($^2\varepsilon$) in permil (‰) units. The hydrogen isotope fractionation between growth water and BP lipids ($^2\varepsilon_{L/W}$) is calculated as:

Eq. (5 a, b)

$$^2\alpha_{L/W} = \frac{^2H/\ ^1H_{BP}}{^2H/\ ^1H_{Water}}$$

$$^2\varepsilon_{L/W}\ (‰) = (\ ^2\alpha_{L/W} - 1)$$

Corrected δ^2H_{BP} values and resulting $^2\varepsilon_{L/W}$ fractionation factors from biological replicates ($n \geq 1$) and analytical replicates ($n \geq 3$) were averaged for each experimental condition. All averages are weighted means of individual measurements ($1/\sigma^2$ weights) to account for the amplitude-dependent range in uncertainties. The reported error estimate of each average is the larger of the standard deviation of all replicates or the propagated uncertainty from individual measurements. Abundance weighted averages for δ^2H_{BP} and $^2\varepsilon_{L/W}$ values include all BPs with relative abundance > 5%.

The ring difference ($\Delta\varepsilon$/ring), or changes in $^2\varepsilon_{L/W}$ with increasing number of ring structures is calculated for all pairwise combinations of $^2\varepsilon_{L/W}$ after Leavitt et al., (2023) where X and Y refer to the ring number of BP moieties and X > Y:

Eq. (6)

$$\frac{\Delta\varepsilon}{ring}(‰) = \frac{^2\varepsilon_{L/W}(X) - \ ^2\varepsilon_{L/W}(Y)}{(X-Y)}$$

Raw data archived on Zenodo (Harris 2025); code for all data manipulations and statistical analyses is available on GitHub (https://github.com/carolynnharris/Saci_Enviro_d2H).

3. Results

We examined how temperature, pH, shaking rate, O_2 availability, and electron donor (sucrose) flux influence H-isotope fractionation in *S. acidocaldarius* through a series of batch, fed-batch, and chemostat experiments. Details of the growth responses and lipid iGDGT profile responses to these conditions can be found in Cobban et al., (2020) and Zhou et al., (2019). In brief, each environmental condition independently influences growth rate, the relative abundance of many subsets of iGDGT core lipids, and the RI-GDGT (Cobban et al. 2020; Zhou et al. 2020) (**Table 1, FIG 2A-E, S1**).

Here, we show that each environmental condition also influences the relative abundance of BP lipids and the RI-BP (**Table 2**, **FIG. 2F-O**). Among all samples, the relative abundance of biphytanes averaged 13%, 30%, 49%, 7% for BP-0, -1, -2, and -3, respectively; BP-3 was the least abundant and was not measurable in some samples. RI-BP ranged from 1.01 to 2.04 and, as expected, was positively correlated with RI-GDGT (R^2 = 0.52, p = 0.001, **FIG. S2**). Among all samples, the abundance weighted mean δ^2H_{BP} values range from -276 to -225 ‰ and were consistently depleted in ^2H relative to growth water, corresponding to $^2\varepsilon_{L/W}$ values from -230 to -180 ‰ (**Table 2, FIG. 2P-T**).

Despite significant effects on growth rate and lipid cyclization, individual environmental parameters had minimal impact on $^2\varepsilon_{L/W}$ values, which spanned a range of 44, 31, 15, 21, and 25 ‰ in the temperature, pH, shaking rate, O_2 availability, and electron donor flux experiments, respectively. We observed a weak linear relationship between environmental conditions and $^2\varepsilon_{L/W}$ only in the electron donor flux experiment, where larger doubling times are associated with slightly less negative $^2\varepsilon_{L/W}$ values (smaller offset from water) (R^2 = 0.89, p = 0.22, slope = 0.72 ± 0.25 ‰/ hour) (**FIG. 2T**).

In the batch and fed-batch experiments, $^2\varepsilon_{L/W}$ values for individual BPs showed no consistent pattern with increasing number of cyclic moieties and the ring difference (Δε/ring) varied widely in direction and magnitude among all treatments (-39 to +24 ‰) (**Table 2**, **FIG. 3A-D, S3A-D**). The variability in mean Δε/ring was smaller, though still not of uniform direction, with values ranging from -5.4 to +10.2 ‰ (**Table 2, FIG. S4A-D**). In contrast, $^2\varepsilon_{L/W}$ values in the chemostat experiment generally increased with the number of cyclic moieties, showing offsets of 3.7, 4.1, and 10.1 ‰ for BP-1, BP-2, and BP-3 relative to BP-0 (**Table 2, FIG. 3E, S3E**). Similarly, the mean ring difference (Δε/ring) was uniformly positive and showed little variation among doubling times, ranging from 4.9 to 9.2 ‰ (**Table 2, FIG. S4E**). On average in continuous culture, each additional ring contributes a 7.4 ± 2.2 ‰ increase to biphytane $^2\varepsilon_{L/W}$.

Correlation matrices show the linear relationship between each environmental condition, growth parameters (doubling time and maximum OD_{600}), mean lipid cyclization indices (RI-BP and RI-GDGT), Δε/ring and abundance weighted $^2\varepsilon_{L/W}$ values for each environmental condition experiment (**FIG. 4**). These plots further demonstrate that the minimal variation in $^2\varepsilon_{L/W}$ observed within each experiment

is not related to variation in the experimentally manipulated environmental conditions or any other measured parameter.

To explore the possibility that lipid/water fractionation is related to optimal growth, we relate abundance weighted mean $^{2}\varepsilon_{L/W}$ values to doubling time for each environmental condition (**FIG. 5A-E**). To allow for comparisons among all environmental conditions, we also relate $^{2}\varepsilon_{L/W}$ to doubling time for all experiments combined. In this pooled dataset, abundance weighted mean $^{2}\varepsilon_{L/W}$ values range from -230 to -180 ‰ (mean = -204 ± 12 ‰, based on 22 biological replicates; **Table 2**) and showed no correlation to doubling time (**FIG. 5F**, $R^2 = 0.0$, $p = 0.97$), indicating a decoupling between lipid/water fractionation and growth rate.

4. Discussion

4.1 Effect of environmental conditions on archaeal lipid $^{2}\varepsilon_{L/W}$ values

The primary goal of this work was to investigate the impact of environmental conditions on lipid/water fractionation in archaeal lipids, which relates to their potential as archives of hydroclimate across space and time. The conditions tested in this study were chosen to encompass the natural conditions of thermoacidophilic archaea, which are globally distributed in hot, acidic features including fumaroles (steam saturated discharges) as geysers and pools in the terrestrial environment, and hydrothermal vents in the marine environment (Lewis et al. 2021). Both realms experience steep and rapidly changing gradients in temperature, pH, oxygen, and dissolved solute concentrations, which can disturb ecological niches (Reysenbach and Cady 2001). As a result, Archaea have adapted to or evolved strategies to mitigate these challenges (Auernik et al. 2008; Lewis et al. 2021).

In *S. acidocaldarius*, our experimental manipulations of temperature, pH, shaking rate, electron acceptor (O_2) availability, and electron donor (sucrose) flux elicited a 20-fold change in growth rate and 2-fold change in mean biphytane cyclization (RI-BP), but $^{2}\varepsilon_{L/W}$ values were largely invariant (-204 ± 12 ‰, n = 22). This finding is consistent with previous studies that show archaeal lipids are consistently ^{2}H-depleted relative to source water and display a narrow range of $^{2}\varepsilon_{L/W}$ values despite considerable variation in taxonomy, metabolic mode, and growth conditions (Kaneko et al. 2011; Dirghangi and Pagani 2013; Lengger et al. 2020; Wu et al. 2020; Leavitt et al. 2023; Rhim et al. 2024) (**FIG 6**).

In heterotrophic archaea, lipid-bound H can originate from water or the organic substrate used for growth, with intracellular hydride carriers, such as NADPH, mediating the incorporation of H from both sources into lipids (Zhang et al. 2009a; Dirghangi and Pagani 2013; Wijker et al. 2019). In heterotrophs, the NADPH incorporated into lipid products inherits some H from the available organic substrate(s). While there are several potential mechanisms by which each environmental stressor tested here could influence lipid/water fractionation in archaea, our data suggest these processes

either do not occur or are insufficient to cause a measurable effect. Temperature, pH, oxygen levels, and nutrient availability are known to trigger physiological responses in archaea, including changes in growth rates, membrane lipid composition, and enzyme activity (Siliakus et al. 2017; Bischof et al. 2019; Cobban et al. 2020; Zhou et al. 2020). Enzyme kinetics, which are influenced by growth temperature and oxidative stress (Jia et al. 2015), could affect lipid/water fractionation if the enzyme catalyzing hydrogen transfer is associated with a significant isotope effect (Zhang et al. 2009a). High temperatures and low pH reduce water exchange across archaeal membranes to prevent osmotic stress (Siliakus et al. 2017), which could enrich the intracellular water in ^{2}H and potentially reduce apparent lipid/water fractionation (Sachs and Schwab 2011). Additionally, changes in electron donor availability can shift the pathway by which NADPH is reduced, which could influence the $\delta^{2}H$ composition of NADPH, which ultimately supplies protons to lipid products (Thauer et al. 2008; Spaans et al. 2015). For example, methanogenic archaea switch between the reductive acetyl-CoA and F_{420}-dependent hydrogenase systems depending on if electron donors (H_2 or formate) are abundant or limiting (Thauer et al. 2008). Despite these possible mechanisms, lipid/water fractionation in *S. acidocaldarius* remains largely invariant in each experiment, indicating that these processes either do not occur or are not significant enough to alter fractionation under the tested conditions. An alternative hypothesis is that *S. acidocaldarius* maintains a constant internal metabolic balance, particularly in NADPH production and utilization, regardless of external conditions.

Physiological responses to stressors impact growth rate and examining $^{2}\varepsilon_{L/W}$ values in response to optimal vs. suboptimal growth may provide a more coherent explanation for the non-linear patterns we observe across the environmental conditions tested. The $^{2}\varepsilon_{L/W}$ values for *S. acidocaldarius*, however, are not correlated to growth rate in any single environmental condition experiment or when data for all conditions are pooled. This finding suggests that cells maintain stable internal metabolic processes resulting in a consistent H-balance over a range of growth rates and is consistent with the theory that a constant lipid/water fractionation is a feature of an imperturbable central energy metabolism (Leavitt et al. 2023; Rhim et al. 2024). *S. acidocaldarius*, like most archaea, employs energy-efficient metabolic strategies (Wakagi and Oshima 1987; Liu et al. 2021), possibly as an adaptation to energy-limiting environments (Valentine 2007; Auernik et al. 2008). In tightly controlled metabolic pathways, the balance between supply and use of NADPH reducing power appears to remain constant, even under energy-stress conditions. Previous research suggests archaea may exist in a permanent state of NADPH deficiency such that all NADPH is immediately used for biosynthesis with little to no flux from NADPH back to NADH (Leavitt et al. 2023). This efficiency in NADPH use may explain why changing growth rates do not impact kinetic isotope effects associated with biosynthesis and hydride exchange. NADPH deficiency (deemed NADPH flux imbalance by Wijker et al., 2019) is associated with energy limitation, and can provide a framework to relate patterns in $^{2}\varepsilon_{L/W}$ values to the fluxes of H through dehydrogenase and transhydrogenase enzymes. Indeed, NADPH flux imbalance may explain why all archaea (to-date) and autotrophic and obligately anaerobic bacteria display negative $^{2}\varepsilon_{L/W}$ values of similar magnitude (Zhang et al. 2009a; Osburn et

al. 2016; Wijker et al. 2019; Rhim et al. 2024). This similarity is striking given that fatty acids and isoprenoid GDGTs are formed via different biosynthetic pathways and suggests that the ultimate control on $^{2}\varepsilon_{L/W}$ values may be related to free energy yields (Rhim et al. 2024).

Both the O_2 availability and sucrose flux experiments test the hypothesis that energy limitation – either terminal electron acceptor or donor – can alter $^{2}\varepsilon_{L/W}$ values in archaea. These experiments produced the largest range in doubling times (2 to 50 hours and 7 to 44 hours in the O_2 availability and electron donor experiments, respectively); yet $^{2}\varepsilon_{L/W}$ values remained fairly consistent (-217 to -196 ‰ and -276 to -244 ‰, respectively). *N. maritimus* is the only other archaeon in which the relationship between electron donor (ammonium) flux and lipid/water fractionation was examined (Leavitt et al. 2023) *N. maritimus* similarly exhibited no significant correlation between a three-fold change in doubling time and $^{2}\varepsilon_{L/W}$ values ($R^2 = 0.22$, $p = 0.07$, slope = 0.18 ± 0.09 ‰/ hour) (Leavitt et al. 2023). The authors speculate this strain maintains a consistent H-balance over a range of electron donor fluxes as an adaptation that allows cells to perform nitrification with energy-efficient CO_2 fixation in oligotrophic environments (Leavitt et al. 2023). These findings suggest that archaea with diverse physiologies (e.g., heterotrophy vs. chemoautotrophy, extremophily vs. mesophily) maintain a constant lipid-to-water fractionation that is minimally affected by free energy availability and may reflect the fact that Archaea are adapted to chronic energy limitation (Valentine 2007; Auernik et al. 2008). This stability may reflect tightly regulated physiological processes, such as isoenzyme switching and modulation of enzyme activities, which help maintain metabolic homeostasis under both optimal and sub-optimal growth conditions (Bräsen et al. 2014). In contrast, in bacteria and some planktonic eukaryotes faster growth is associated with larger lipid/water fractionation (Schouten et al. 2006; Zhang et al. 2009b; Sachs and Schwab 2011) and $^{2}\varepsilon_{L/W}$ values for Bacteria are influenced by electron donor flux (Zhang et al. 2009a; Osburn et al. 2016; Wijker et al. 2019).

The only other study in archaea to examine the relationship between environmental conditions and lipid/water fractionation cultured the halophilic heterotrophic archaeon, *H. marismortui* (which produces archaeol diethers), under varying temperatures and salinities when grown on complex rich medium (Dirghangi and Pagani 2013). The resulting $^{2}\varepsilon_{Archaeol/W}$ values are relatively invariant (ranging from -126 to -143 ‰; more enriched than our observations for *S. acidocaldarius*) and are decoupled from growth rate (**FIG. S5;** $R^2 = 0.07$, $p = 0.7$, slope = 0.85 ± 1.84 ‰ / hour; Dirghangi and Pagani 2013), providing more evidence that archaea maintain a stable internal H-balance across a range of growth conditions.

The impact of growth phase on H-isotope dynamics has not been studied in depth. The batch and fed-batch experiment techniques used here for *S. acidocaldarius* and in the *H. marismortui* study integrate across growth stages, whereas the chemostat electron donor flux experiments for *S. acidocaldarius* and *N. maritimus* achieve constant growth rates. A recent study grew *A. fulgidus* in batch cultures and found that $^{2}\varepsilon_{L/W}$ values were more depleted (larger offset from water) during exponential phase relative to stationary phase (Rhim et al. 2024). This pattern was consistent

between heterotrophic and autotrophic experiments. The culture conditions in Rhim et al. resulted in a threefold difference in growth rates (similar change to the *N. maritimus* study, but much smaller range than the 20-fold change we report for *S. acidocaldarius* here) and a 50 ‰ change in $^{2}\varepsilon_{L/W}$ values (-280 ‰ to -230 ‰). Rhim and coauthors conclude that both metabolic mode (heterotrophic vs. autotrophic growth) and growth phase impact $^{2}\varepsilon_{L/W}$ values, though the total variance among all treatments was small and overlaps which ranges reported for other archaea (Rhim et al. 2024).

4.2 Effect of biphytane ring number on archaeal lipid $^{2}\varepsilon_{L/W}$ values

Stoichiometric modeling predicts that BPs with more rings incorporate less of the highly-fractionated hydrogen donated through GGR reduction, a process where the enzyme geranyl-geranyl reductase (GGR) catalyzes the reduction of double bonds in isoprenoid chains, thereby affecting the isotopic composition of the resulting lipids (Leavitt et al. 2023). Interestingly, in our *S. acidocaldarius* work, this stepwise enrichment is only seen in the chemostat experiments, where each additional ring contributes 7.4 ± 2.2 ‰ to biphytane $^{2}\varepsilon_{L/W}$ values. In the batch and fed-batch experiments, there is no consistent dependence of $^{2}\varepsilon_{L/W}$ values on the number of biphytane moieties. In particular, the Δε/ring trends differ between the shaking rate and O_2 availability experiments, which likely reflects the fact that shaking rate can also impart stress via physical agitation in addition to increasing oxygenation of microbial media (Cobban et al. 2020).

iGDGT-derived BPs extracted from marine sediments also lack a clear stepwise enrichment with increasing ring moieties (Kaneko et al. 2011), but this likely occurs because sediments integrate lipids synthesized by different populations of archaea that are either growing on multiple substrates or in different water masses (Kaneko et al. 2011). It is less clear why the pure *S. acidocaldarius* batch and fed-batch cultures do not display a ring-specific pattern, though it perhaps relates to variations in biosynthetic fractionations accompanying changes in lipid biosynthesis across the growth phases (Elling et al. 2014). Considering all the available data, this enrichment pattern appears only minimally affected by differences in growth rate and metabolism, as the magnitude of per-ring increase in $^{2}\varepsilon_{L/W}$ value is similar for *Sulfolobus* sp. (Kaneko et al. 2011), *S. acidocaldarius* (chemostat experiment in this study), and *N. maritimus* (Leavitt et al. 2023), which collectively represent a 5-fold range of growth rates, and a variety of metabolisms and carbon substrates (*Sulfolobus* sp. = yeast extract + O_2; *S. acidocaldarius* = sucrose + O_2; *N. maritimus* = chemoautotroph on NH_4 + O_2). The magnitude of this stepwise enrichment, however, is small and would likely have a minor impact (usually < 10 ‰) on the abundance weighted mean $^{2}\varepsilon_{L/W}$ value even in cases where the BP Ring Index was markedly different among samples.

4.3 Archaeal lipid $^{2}\varepsilon_{L/W}$ as a function of central metabolism

The *S. acidocaldarius* $^{2}\varepsilon_{L/W}$ values we report are broadly similar to results from previous experimental investigations of the *Sulfolobus* genus cultured heterotrophically. When grown at 75 °C and pH 2 on yeast extract, a *Sulfolobus* strain displayed $^{2}\varepsilon_{L/W}$ values from -213 to -161 ‰ for BP-0 to -4

(abundance weighted mean = -180 ‰ (Kaneko et al. 2011) vs. -204 ± 12 ‰ for *S. acidocaldarius* here). In another study, *Sulfolobus solfataricus* grown at 76 °C and pH 3.5 on glutamate displayed more enriched $^{2}\varepsilon_{L/W}$ values, averaging -134 ‰ when intact iGDGT-1 and -2 were analyzed (Lengger et al. 2020). The difference in $^{2}\varepsilon_{L/W}$ values may in part be due to the structures analyzed. Lengger and colleagues analyzed intact iGDGTs including the glycerols which may enrich the $\delta^{2}H_{iGDGT}$ composition, though the different substrate may also play a role (Lengger et al. 2020). Glutamate, an amino acid, is a more complex substrate than simple sugars (such as sucrose) and primarily enters the *Sulfolobus* central metabolism through the TCA cycle (Quehenberger et al. 2019). Simple sugars enter metabolism primarily through the Entner-Doudoroff pathway, which converts the sugar to intermediates that feed into the TCA cycle (Quehenberger et al. 2019).

When *S. acidocaldarius* is grown heterotrophically on a simple sugar (glucose), the weighted mean $\delta^{2}H$ composition of biphytane lipids is strongly correlated with $\delta^{2}H_{Water}$, indicating a strong first-order control (see *Supplementary Materials*, **FIG. S6**). A simple isotope mass balance model (**Eq. S1**) suggests water contributes at least 56 ± 1% of the total H flux to lipids (**FIG. S7**). Further experimental work and complementary isotope flux models are needed to determine the specific pathways (and associated isotope effects) used during iGDGT synthesis in *S. acidocaldarius* (Harris et al. 2022).

Autotrophic archaea that produce iGDGTs, however, source their entire H budget to lipids from water in the growth environment and show more negative $^{2}\varepsilon_{L/W}$ values than those we observe for *S. acidocaldarius*. In the marine chemoautotroph, *N. maritimus*, grown in continuous culture, BP/water fractionation ranged from -272 to -260 ‰ (Leavitt et al. 2023). Similarly, BP/water fractionations for a metabolically-flexible archaeon, *Archaeoglobus fulgidus*, ranged from -280 to -226 ‰ when cultured with several unique carbon substrates and electron donor/acceptor pairs (Rhim et al. 2024). This difference may be driven by the distinct metabolic modes used (e.g., autotrophy vs. heterotrophy) and/or by unique metabolic pathways that employ various intracellular hydride carriers and reductants to bring H's to the lipid sites, which could generate different net biosynthetic fractionations. Metabolic flux models suggest that in autotrophic archaea (e.g., *N. maritimus*), H-isotope fractionation due to the electron transport chain and NADPH generation result in more depleted lipids than for heterotrophic archaea, such as *Sulfolobus* species, because the source of NADPH impacts $^{2}\varepsilon_{L/W}$ values (Leavitt et al. 2023). In both heterotrophic and aerobic archaea, most NADPH is generated by glucose dehydrogenase and potentially glyceraldehyde dehydrogenase from the Entner-Doudoroff pathway (Nunn et al. 2010; Bräsen et al. 2014).

Overall, the range of $^{2}\varepsilon_{L/W}$ values in Archaeal lipids is narrower than the ranges observed in Bacteria or Eukarya (**FIG. 6**). While the sample size for Bacteria and Eukarya are two-fold and four-fold larger than for Archaea, respectively, Bartlett's test for homogeneity of variances confirm that Archaeal $^{2}\varepsilon_{L/W}$ values have smaller variance compared to Eukarya ($K^{2}_{(1)} = 16.4$, $p < 0.0001$) and Bacteria ($K^{2}_{(1)} = 118.5$, $p < 0.0001$) after accounting for sample size. Reported $^{2}\varepsilon_{L/W}$ values for bacterial fatty acids vary over 600 ‰ and include large negative and large positive values (Campbell et al. 2009; Zhang et

al. 2009a; Osburn et al. 2016; Wijker et al. 2019; Rhim et al. 2024). In Eukarya, $^{2}\varepsilon_{L/W}$ values are uniformly negative and span over 300 ‰, though certain lipid classes group together (Sessions et al. 1999; Zhang and Sachs 2007; Sachs et al. 2016). Lipids that are formed via the same biosynthetic pathway (e.g., acetogenic or isoprenoid pathway) tend to occupy distinct ranges of $^{2}\varepsilon_{L/W}$ (Rhim et al. 2024). Isoprenoid lipids produced via the MVA pathway in eukaryotes have similar $^{2}\varepsilon_{L/W}$ values to iGDGT-derived biphytanes in archaea (Rhim et al. 2024). This similarity suggests that the MVA pathway used for isoprenoid lipid biosynthesis has a large net fractionation in both domains of life.

4.4 Applications and Conclusion

Our calibration of biphytane $\delta^{2}H$ composition as a proxy for the $\delta^{2}H$ of environmental water in *S. acidocaldarius* has significant implications for paleohydroclimate and paleoecology reconstructions. First, this calibration may enable hydroclimate factors like precipitation, elevation, and seasonality to be reconstructed for environments that do not contain traditionally analyzed lipid biomarkers (e.g., plant waxes) – this includes extreme environments that do not support plant growth (e.g., terrestrial hydrothermal systems, salars, and hyperarid regions). Archaeal lipid $\delta^{2}H$ values will be most powerful as a proxy in cases where a single-substrate source is a reasonable assumption.

Second, biphytane $\delta^{2}H$ composition could be applied to marine or lacustrine sedimentary archives where multiple sources of organic matter are suspected, such as a mix of plant waxes representing *in situ* marine/ aquatic production and allochthonous terrestrial production (e.g., aeolian deposition). In this case, plant wax $\delta^{2}H$ values would reflect a mixture of growth waters (marine/lake water and soil water). In contrast, iGDGTs are likely derived solely from archaea living in the overlying water column with few potential terrestrial sources and thus the $\delta^{2}H$ composition of iGDGTs would only reflect marine/lake water (Pearson and Ingalls 2013).

Here, we show that in the model thermoacidophile *S. acidocaldarius* grown on simple sugars, lipid-water fractionation ($^{2}\varepsilon_{L/W}$) is not dependent on any of the environmental conditions tested or on growth rate. This finding suggests that *S. acidocaldarius* may have evolved stable metabolisms that exist in a constant NADPH deficit, possibly reflecting adaptation to energy-limiting environments. We conclude that *S. acidocaldarius* will likely demonstrate reliably invariant lipid/water fractionation regardless of growth rate, nutrient status, or energy availability, and that lipid/water fractionation may be more constant for certain archaeons than for phototrophic eukaryotes. For both domains, however, there is more variability in lipid/water fraction relative to the spatial and temporal variability in precipitation $\delta^{2}H$ values, and more research is needed to understand the sources of this variation so that it can be accounted for in proxy applications.

This calibration underscores the potential for archaeal lipid $\delta^{2}H$ composition as a proxy for past hydroclimates that could complement or be used independently of eukaryotic lipid $\delta^{2}H$ composition. Future research should focus on exploring the effects of growth phase and metabolic

pathways on lipid/water fractionation in *S. acidocaldarius* and other archaeal species. Expanding these investigations to include more diverse environmental conditions, such as varying carbon substrates or mixed microbial communities, could further validate the consistency of $^{2}\varepsilon_{L/W}$ values and refine its utility as a hydrological proxy. Integrating isotope flux models with experimental data such as those generated here, will allow us to better elucidate the specific biochemical pathways responsible for the observed fractionation patterns in domain Archaea.

Acknowledgements

This research was supported by research grant NSF EAR #1928303940 (WDL, SHK); Simons Foundation Award #623881 (WDL); Dartmouth College (WDL); National Aeronautics and Space Administration (NASA) New Hampshire Space Grant (NASA-SSW-80NSSC19K0539); Deutsche Forschungsge-meinschaft grant 441217575 (F.J.E.). The authors thank the CU Boulder Earth Systems Stable Isotope Lab (CUBES-SIL) Core Facility (RRID:SCR_019300) for analytical contributions; B. Chiu (then at Dartmouth), J. Blewett (then at Harvard), S. Carter (Harvard), and A. Maloney (CU Boulder) for expert laboratory support; Simon D. Kelly from International Atomic Energy Agency, Vienna for measuring the $\delta^{2}H$ composition of carbon substrates; and all members of the Leavitt lab for all their support.

557 References

558 Abrahim A, Cannavan A, Kelly SD (2020) Stable isotope analysis of non-exchangeable hydrogen in
559 carbohydrates derivatised with N-methyl-bis-trifluoroacetamide by gas chromatography –
560 Chromium silver reduction/High temperature Conversion-isotope ratio mass spectrometry
561 (GC-CrAg/HTC-IRMS). Food Chemistry 318:126413.
562 https://doi.org/10.1016/j.foodchem.2020.126413

563 Auernik KS, Cooper CR, Kelly RM (2008) Life in hot acid: pathway analyses in extremely
564 thermoacidophilic archaea. Current Opinion in Biotechnology 19:445–453.
565 https://doi.org/10.1016/j.copbio.2008.08.001

566 Baan J (2024) Understanding the metabolic signal in hydrogen isotope values of plant organic
567 compounds. Thesis der Universitat Basel. https://doi.org/DOI 10.5451/unibas-ep96717

568 Baan J, Holloway-Phillips M, Nelson DB, Kahmen A (2023) Species and biosynthetic effects cause
569 uncorrelated variation in oxygen and hydrogen isotope compositions of plant organic
570 compounds. Geochimica et Cosmochimica Acta 352:1–13.
571 https://doi.org/10.1016/j.gca.2023.04.013

572 Bender, Suess, Chitwood, Bradley (2016) Investigating genetic loci that encode plant-derived
573 paleoclimate proxies. pp PP24B-03

574 Bischof LF, Haurat MF, Hoffmann L, et al (2019) Early Response of Sulfolobus acidocaldarius to
575 Nutrient Limitation. Front Microbiol 9:3201. https://doi.org/10.3389/fmicb.2018.03201

576 Bräsen C, Esser D, Rauch B, Siebers B (2014) Carbohydrate Metabolism in Archaea: Current
577 Insights into Unusual Enzymes and Pathways and Their Regulation. Microbiol Mol Biol Rev
578 78:89–175. https://doi.org/10.1128/MMBR.00041-13

579 Brock TD, Brock KM, Belly RT, Weiss RL (1972) Sulfolobus: A new genus of sulfur-oxidizing bacteria
580 living at low pH and high temperature. Archiv Mikrobiol 84:54–68.
581 https://doi.org/10.1007/BF00408082

582 Campbell BJ, Li C, Sessions AL, Valentine DL (2009) Hydrogen isotopic fractionation in lipid
583 biosynthesis by H2-consuming Desulfobacterium autotrophicum. Geochimica et
584 Cosmochimica Acta 73:2744–2757. https://doi.org/10.1016/j.gca.2009.02.034

585 Cobban A, Zhang Y, Zhou A, et al (2020) Multiple environmental parameters impact core lipid
586 cyclization in Sulfolobus acidocaldarius. Environmental Microbiology 1–28

587 Dawson D, Grice K, Wang SX, et al (2004) Stable hydrogen isotopic composition of hydrocarbons in
588 torbanites (Late Carboniferous to Late Permian) deposited under various climatic
589 conditions. Organic Geochemistry 35:189–197.
590 https://doi.org/10.1016/j.orggeochem.2003.09.004

591 Dawson KS, Osburn MR, Sessions AL, Orphan VJ (2015) Metabolic associations with archaea drive
592 shifts in hydrogen isotope fractionation in sulfate-reducing bacterial lipids in cocultures
593 and methane seeps. Geobiology 13:462–477. https://doi.org/10.1111/gbi.12140

De Rosa M, Gambacorta A (1988) The lipids of archaebacteria. Progress in Lipid Research 27:153–175. https://doi.org/10.1016/0163-7827(88)90011-2

Dirghangi SS, Pagani M (2013) Hydrogen isotope fractionation during lipid biosynthesis by Haloarcula marismortui. Geochimica et Cosmochimica Acta 119:381–390. https://doi.org/10.1016/j.gca.2013.05.023

Elling FJ, Könneke M, Lipp JS, et al (2014) Effects of growth phase on the membrane lipid composition of the thaumarchaeon Nitrosopumilus maritimus and their implications for archaeal lipid distributions in the marine environment. Geochimica et Cosmochimica Acta 141:579–597. https://doi.org/10.1016/j.gca.2014.07.005

Elling FJ, Könneke M, Nicol GW, et al (2017) Chemotaxonomic characterisation of the thaumarchaeal lipidome. Environmental Microbiology 19:2681–2700. https://doi.org/10.1111/1462-2920.13759

Gao L, Edwards EJ, Zeng Y, Huang Y (2014) Major Evolutionary Trends in Hydrogen Isotope Fractionation of Vascular Plant Leaf Waxes. PLoS ONE 9:e112610. https://doi.org/10.1371/journal.pone.0112610

Gat JR (1996) Oxygen and hydrogen isotopes in the hydrologic cycle. Annual Review of Earth and Planetary Sciences 24:225–262. https://doi.org/10.1146/annurev.earth.24.1.225

Harris C (2025) Raw data for Harris et al., 2025 AEM_Sulfolobus acidocaldarius d2H. Zenodo https://zenodo.org/doi/10.5281/zenodo.14743884.

Harris C, Rhim J, Zhang Y, et al (2022) Determining controls on hydrogen isotope fractionation in archaeal tetraether lipids in a thermoacidophilic archaeal heterotroph. In: Goldschmidt2022 abstracts. European Association of Geochemistry, Honolulu, HI, USA

Hayes JM (2001) Fractionation of carbon and hydrogen isotopes in biosynthetic processes. Stable Isotope Geochemistry 43:225–277. https://doi.org/10.2138/gsrmg.43.1.225

Hurley SJ, Elling FJ, Könneke M, et al (2016) Influence of ammonia oxidation rate on thaumarchaeal lipid composition and the TEX86 temperature proxy. Proceedings of the National Academy of Sciences of the United States of America 113:7762–7767. https://doi.org/10.1073/pnas.1518534113

Jia B, Liu J, Van Duyet L, et al (2015) Proteome profiling of heat, oxidative, and salt stress responses in Thermococcus kodakarensis KOD1. Front Microbiol 6:. https://doi.org/10.3389/fmicb.2015.00605

Kaneko M, Kitajima F, Naraoka H (2011) Stable hydrogen isotope measurement of archaeal ether-bound hydrocarbons. Organic Geochemistry 42:166–172. https://doi.org/10.1016/j.orggeochem.2010.11.002

Kopf S, Davidheiser-Kroll B, Kocken I (2021) Isoreader: An R package to read stable isotope data files for reproducible research. JOSS 6:2878. https://doi.org/10.21105/joss.02878

Ladd N, Nelson D, Matthews B, et al (2024) Taxon-specific hydrogen isotope signals in cultures and mesocosms facilitate ecosystem and hydroclimate reconstruction. EarthArXiv. https://doi.org/10.31223/X57T30

Ladd SN, Nelson DB, Bamberger I, et al (2021) Metabolic exchange between pathways for isoprenoid synthesis and implications for biosynthetic hydrogen isotope fractionation. New Phytologist 231:1708–1719. https://doi.org/10.1111/nph.17510

Leavitt WD (2016) The Inner Lives of Archaea: the hydrogen isotopic composition of Archaeal lipids as a proxy of metabolic state

Leavitt WD, Kopf SH, Weber Y, et al (2023) Controls on the hydrogen isotope composition of tetraether lipids in an autotrophic ammonia-oxidizing marine archaeon. Geochimica et Cosmochimica Acta 352:194–210. https://doi.org/10.1016/j.gca.2023.04.033

Leavitt WD, Murphy SJL, Lynd LR, Bradley AS (2017) Hydrogen isotope composition of Thermoanaerobacterium saccharolyticum lipids: Comparing wild type with a nfn-transhydrogenase mutant. Organic Geochemistry 113:239–241. https://doi.org/10.1016/j.orggeochem.2017.06.020

Lengger SK, Weber Y, Taylor KWR, et al (2020) Determination of the d2H values of high molecular weight lipids by high temperature GC coupled to isotope ratio mass spectro. Rapid Communications in Mass Spectrometry

Lewis AM, Recalde A, Bräsen C, et al (2021) The biology of thermoacidophilic archaea from the order Sulfolobales. FEMS Microbiology Reviews 1–60. https://doi.org/10.1093/femsre/fuaa063

Liu J, An Z (2019) Variations in hydrogen isotopic fractionation in higher plants and sediments across different latitudes: Implications for paleohydrological reconstruction. Science of The Total Environment 650:470–478. https://doi.org/10.1016/j.scitotenv.2018.09.047

Liu L-J, Jiang Z, Wang P, et al (2021) Physiology, Taxonomy, and Sulfur Metabolism of the Sulfolobales, an Order of Thermoacidophilic Archaea. Front Microbiol 12:768283. https://doi.org/10.3389/fmicb.2021.768283

Love GD, Zumberge JA (2021) Emerging Patterns in Proterozoic Lipid Biomarker Records, 1st edn. Cambridge University Press

Maloney AE, Shinneman ALC, Hemeon K, Sachs JP (2016) Exploring lipid 2H/1H fractionation mechanisms in response to salinity with continuous cultures of the diatom Thalassiosira pseudonana. Organic Geochemistry 101:154–165. https://doi.org/10.1016/j.orggeochem.2016.08.015

McFarlin JM, Axford Y, Masterson AL, Osburn MR (2019) Calibration of modern sedimentary δ2H plant wax-water relationships in Greenland lakes. Quaternary Science Reviews 225:105978. https://doi.org/10.1016/j.quascirev.2019.105978

Nunn CEM, Johnsen U, Schönheit P, et al (2010) Metabolism of Pentose Sugars in the Hyperthermophilic Archaea Sulfolobus solfataricus and Sulfolobus acidocaldarius. Journal of Biological Chemistry 285:33701–33709. https://doi.org/10.1074/jbc.M110.146332

Osburn MR, Dawson KS, Fogel ML, Sessions AL (2016) Fractionation of hydrogen isotopes by sulfate- and nitrate-reducing bacteria. Frontiers in Microbiology 7:1–16. https://doi.org/10.3389/fmicb.2016.01166

Pearson A, Ingalls AE (2013) Assessing the use of archaeal lipids as marine environmental proxies. Annual Review of Earth and Planetary Sciences 41:359–384. https://doi.org/10.1146/annurev-earth-050212-123947

Pilecky M, Kainz MJ, Wassenaar LI (2024) Exploring hydrogen isotope fractionation in lipid biomolecules of freshwater algae: implications for ecological and paleoenvironmental studies. Isotopes in Environmental and Health Studies 60:585–595. https://doi.org/10.1080/10256016.2024.2419880

Quehenberger J, Albersmeier A, Glatzel H, et al (2017) Sulfolobus – A Potential Key Organism in Future Biotechnology. Frontiers in Microbiology 301:56–67. https://doi.org/10.1016/j.jbiotec.2019.04.028

Quehenberger J, Albersmeier A, Glatzel H, et al (2019) A defined cultivation medium for Sulfolobus acidocaldarius. Journal of Biotechnology 301:56–67. https://doi.org/10.1016/j.jbiotec.2019.04.028

Quehenberger J, Pittenauer E, Allmaier G, Spadiut O (2020) The influence of the specific growth rate on the lipid composition of Sulfolobus acidocaldarius. Extremophiles 24:413–420. https://doi.org/10.1007/s00792-020-01165-1

Reysenbach A-L, Cady SL (2001) Microbiology of ancient and modern hydrothermal systems. Trends in Microbiology 9:79–86. https://doi.org/10.1016/S0966-842X(00)01921-1

Rhim JH, Kopf S, McFarlin J, et al (2024) Metabolic imprints in the hydrogen isotopes of Archaeoglobus fulgidus tetraether lipids. Geochimica et Cosmochimica Acta 386:196–212. https://doi.org/10.1016/j.gca.2024.09.032

Sachs J (2014) Hydrogen Isotope Signatures in the Lipids of Phytoplankton. In: Treatise on Geochemistry. Elsevier, pp 79–94

Sachs JP, Kawka OE (2015) The influence of growth rate on 2H/1H fractionation in continuous cultures of the coccolithophorid Emiliania huxleyi and the diatom Thalassiosira pseudonana. PLoS ONE 10:1–27. https://doi.org/10.1371/journal.pone.0141643

Sachs JP, Maloney AE, Gregersen J, Paschall C (2016) Effect of salinity on 2H/1H fractionation in lipids from continuous cultures of the coccolithophorid Emiliania huxleyi. Geochimica et Cosmochimica Acta 189:96–109. https://doi.org/10.1016/j.gca.2016.05.041

Sachs JP, Schwab VF (2011) Hydrogen isotopes in dinosterol from the Chesapeake Bay estuary. Geochimica et Cosmochimica Acta 75:444–459. https://doi.org/10.1016/j.gca.2010.10.013

Sachse D, Billault I, Bowen GJ, et al (2012) Molecular paleohydrology: Interpreting the hydrogen-isotopic composition of lipid biomarkers from photosynthesizing organisms. Annual Review of Earth and Planetary Sciences 40:221–249. https://doi.org/10.1146/annurev-earth-042711-105535

Schouten S, Hopmans EC, SchefuB E, Sinninghe Damsté JS (2002) Distributional variations in marine crenarchaeotal membrane lipids: a new tool for reconstructing ancient sea water temperatures? Earth and Planetary Science Letters 265–274. https://doi.org/10.5642/aliso.19881201.09

Schouten S, Hopmans EC, Sinninghe Damsté JS (2013) The organic geochemistry of glycerol dialkyl glycerol tetraether lipids: A review. Organic Geochemistry 54:19–61. https://doi.org/10.1016/j.orggeochem.2012.09.006

Schouten S, Ossebaar J, Schreiber K, et al (2006) The effect of temperature, salinity and growth rate on the stable hydrogen isotopic composition of long chain alkenones produced by Emiliania huxleyi and Gephyrocapsa oceanica. Biogeosciences 3:113–119. https://doi.org/10.5194/bg-3-113-2006

Sessions AL (2016) Factors controlling the deuterium contents of sedimentary hydrocarbons. Organic Geochemistry 96:43–64. https://doi.org/10.1016/j.orggeochem.2016.02.012

Sessions AL, Burgoyne TW, Schimmelmann A, Hayes JM (1999) Fractionation of hydrogen isotopes in lipid biosynthesis. Organic Geochemistry 30:1193–1200. https://doi.org/10.1016/S0146-6380(99)00094-7

Sessions AL, Jahnke LL, Schimmelmann A, Hayes JM (2002) Hydrogen isotope fractionation in lipids of the methane-oxidizing bacterium Methylococcus capsulatus. Geochimica et Cosmochimica Acta 66:3955–3969. https://doi.org/10.1016/S0016-7037(02)00981-X

Sessions AL, Sylva SP, Summons RE, Hayes JM (2004) Isotopic exchange of carbon-bound hydrogen over geologic timescales. Geochimica et Cosmochimica Acta 68:1545–1559. https://doi.org/10.1016/j.gca.2003.06.004

Siliakus MF, Van Der Oost J, Kengen SWM (2017) Adaptations of archaeal and bacterial membranes to variations in temperature, pH and pressure. Extremophiles 21:651–670. https://doi.org/10.1007/s00792-017-0939-x

Spaans SK, Weusthuis RA, Van Der Oost J, Kengen SWM (2015) NADPH-generating systems in bacteria and archaea. Front Microbiol 6:. https://doi.org/10.3389/fmicb.2015.00742

Thauer RK, Kaster A-K, Seedorf H, et al (2008) Methanogenic archaea: ecologically relevant differences in energy conservation. Nat Rev Microbiol 6:579–591. https://doi.org/10.1038/nrmicro1931

Torres-Romero I, Zhang H, Wijker RS, et al (2024) Hydrogen isotope fractionation is controlled by CO_2 in coccolithophore lipids. Proc Natl Acad Sci USA 121:e2318570121. https://doi.org/10.1073/pnas.2318570121

Valentine DL (2009) Isotopic remembrance of metabolism past. Proceedings of the National Academy of Sciences of the United States of America 106:12565–12566. https://doi.org/10.1073/pnas.0906428106

Valentine DL (2007) Adaptations to energy stress dictate the ecology and evolution of the Archaea. Nature Reviews Microbiology 5:316–323. https://doi.org/10.1038/nrmicro1619

Van de Vossenberg JLCM, Driessen AJM, Konings WN (1998) The essence of being extremophilic: The role of the unique archaeal membrane lipids. Extremophiles 2:163–170. https://doi.org/10.1007/s007920050056

Van Der Meer MTJ, Benthien A, French KL, et al (2015) Large effect of irradiance on hydrogen isotope fractionation of alkenones in Emiliania huxleyi. Geochimica et Cosmochimica Acta 160:16–24. https://doi.org/10.1016/j.gca.2015.03.024

Wakagi T, Oshima T (1987) Energy metabolism of a thermoacidophilic archaebacterium,Sulfolobus acidocaldarius. Origins Life Evol Biosphere 17:391–399. https://doi.org/10.1007/BF02386477

Wijker RS, Sessions AL, Fuhrer T, Phan M (2019) 2H/1H variation in microbial lipids is controlled by NADPH metabolism. Proceedings of the National Academy of Sciences of the United States of America 116:12173–12182. https://doi.org/10.1073/pnas.1818372116

Wolfshorndl M, Danford R, Sachs JP (2019) 2H/1H fractionation in microalgal lipids from the North Pacific Ocean: Growth rate and irradiance effects. Geochimica et Cosmochimica Acta 246:317–338. https://doi.org/10.1016/j.gca.2018.11.027

Wu W, Meador TB, Könneke M, et al (2020) Substrate-dependent incorporation of carbon and hydrogen for lipid biosynthesis by Methanosarcina barkeri. Environmental Microbiology Reports. https://doi.org/10.1111/1758-2229.12876

Yang W, Chen H, Chen Y, et al (2023) Thermophilic archaeon orchestrates temporal expression of GDGT ring synthases in response to temperature and acidity stress. Environmental Microbiology 25:575–587. https://doi.org/10.1111/1462-2920.16301

Zhang X, Gillespie AL, Sessions AL (2009a) Large D/H variations in bacterial lipids reflect central metabolic pathways. Proceedings of the National Academy of Sciences of the United States of America 106:12580–12586. https://doi.org/10.1073/pnas.0903030106

Zhang YG, Pagani M, Wang Z (2016) Ring Index: A new strategy to evaluate the integrity of TEX_{86} paleothermometry. Paleoceanography 31:220–232. https://doi.org/10.1002/2015PA002848

Zhang Z, Sachs JP (2007) Hydrogen isotope fractionation in freshwater algae: I. Variations among lipids and species. Organic Geochemistry 38:582–608. https://doi.org/10.1016/j.orggeochem.2006.12.004

Zhang Z, Sachs JP, Marchetti A (2009b) Hydrogen isotope fractionation in freshwater and marine algae: II. Temperature and nitrogen limited growth rate effects. Organic Geochemistry 40:428–439. https://doi.org/10.1016/j.orggeochem.2008.11.002

Zhou A, Weber Y, Chiu BK, et al (2020) Energy flux controls tetraether lipid cyclization in Sulfolobus acidocaldarius. Environmental Microbiology 22:343–353. https://doi.org/10.1111/1462-2920.14851

Tables

Table 1. Summary of culture conditions and descriptive growth statistics for *S. acidocaldarius* grown over varying environmental conditions. Data for batch and fed-batch environmental condition experiments were initially reported in Cobban et al., (2020), data for chemostat experiment was initially reported in Zhou et al., (2019).

Table 2. Descriptive statistics for biphytanyl (BP) lipids derived from iGDGTs for *S. acidocaldarius* grown under varying environmental conditions. Mean and sd include biological replication (N ≥ 1) and technical replication (e.g., multiple injections, n ≥ 3). *For batch experiments, RPM is shaking rate; for bioreactor experiments, RPM is impellor speed.

Figures

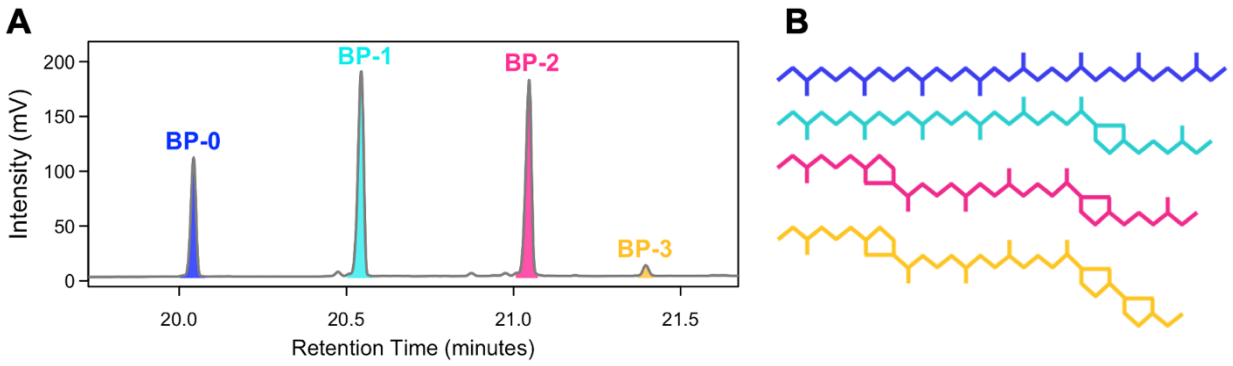

Fig 1. (A) Representative chromatogram of intensity vs. retention time for four iGDGT-derived biphytane (BP) moieties identified in *S. acidocaldarius* biomass that are named for the number of cyclopentane rings they contain. Although a BP-3 peak was detected, in many cases it is present in too low quantities to perform isotopic measurements **(B)** The identity and structure of BP-0 to BP-3.

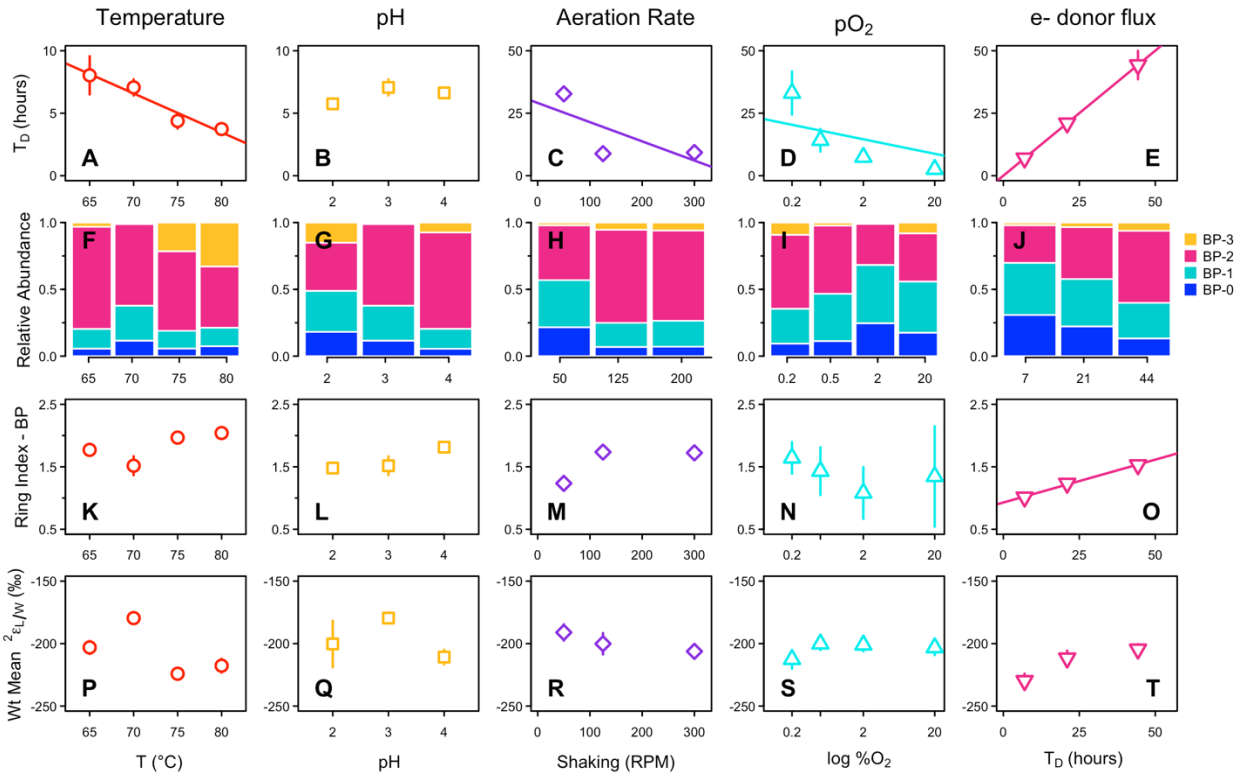

Fig. 2. Results for *S. acidocaldarius* grown under varying environmental conditions. Top row (**A-E**): Doubling time in response to each environmental condition. Second row (**F-J**): Relative abundance of biphytane (BP) lipids derived from iGDGTs. BP-3 was the least abundant and was below the detection limit in some samples. Bars represent the mean across replicates for each treatment level. Third row (**K-O**): Ring Index (RI-BP) of biphytane lipids derived from iGDGTs. Bottom row (**P-T**) The abundance weighted mean H-isotope fractionation ($^{2}\varepsilon_{L/W}$) between growth water and biphytanes. For all rows, points represent the mean and propagated error across biological and technical replicates for each treatment level. In many cases, error bars are smaller than symbols. Only statistically significant regressions are shown ($p < 0.05$).

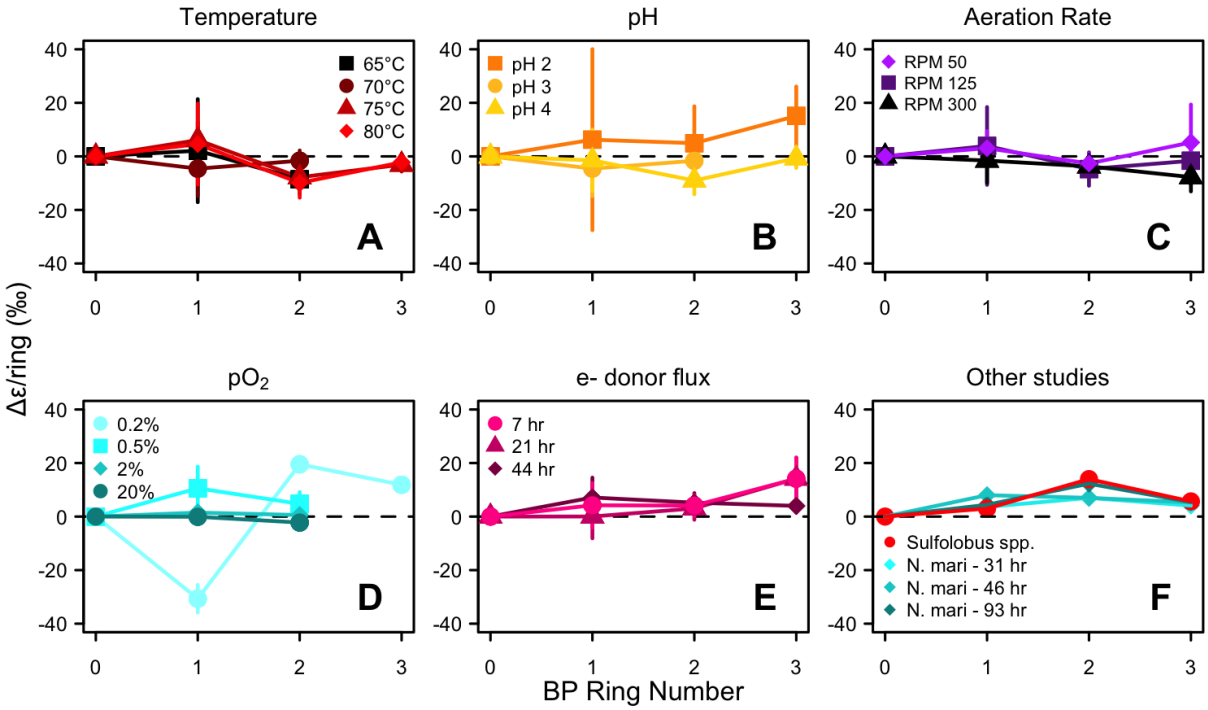

Fig. 3. (**A-E**) Ring difference (Δε/ring, ‰) for individual biphytanes in each environmental condition experiment. BP-0 has a Δε/ring of 0 by definition and is shown for reference. BP-3 was not recovered from every treatment. Note the axes are scaled differently for each plot. Points represent mean of biological and technical replicates for each treatment level. (**F**) Ring difference for biphytanes examined in other studies. Blue diamonds are *N. maritimus* from Leavitt et al., 2023; red squares are *Sulfolobus* sp. from Kaneko et al., 2011. Kaneko et al., also recovered BP-4 from *Sulfolobus* spp. (data not shown); the Δε/ring for BP-4 is 11.7 ‰.

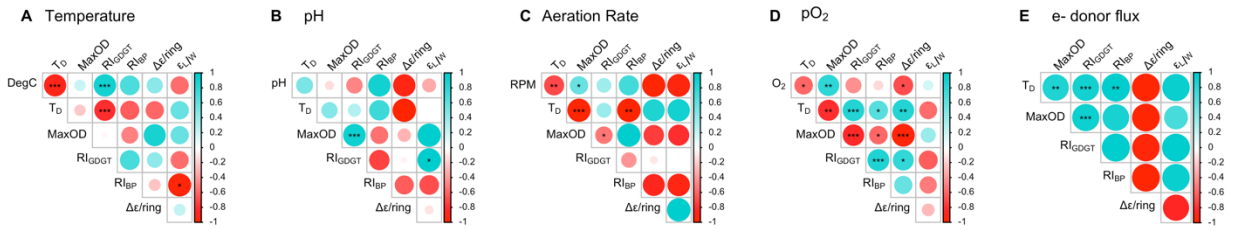

Fig. 4. Correlation matrices showing linear relationships among environmentally manipulated parameters, growth statistics (doubling time (T_D) and maximum OD_{600}), mean cyclization of lipids (RI-GDGT and RI-BP), ring difference, and abundance weighted mean $^2\varepsilon_{L/W}$ for (**A**) temperature, (**B**) pH, (**C**) aeration rate, (**D**) O_2 mixing ratio, and (**E**) electron donor flux. Notably, mean $^2\varepsilon_{L/W}$ values do not show a strong linear correlation to any other measured parameter, indicating that environmental conditions, growth statistics, and mean cyclization do not significantly influence the degree of lipid/water fractionation in *S. acidocaldarius*. Circle color and size indicate the strength and direction (blue = correlated, red = anticorrelated) of the relationship. Significance levels: * $p < 0.05$, ** $p < 0.001$, *** $p < 0.0001$. Circles without a star indicate the relationship is not statistically significant.

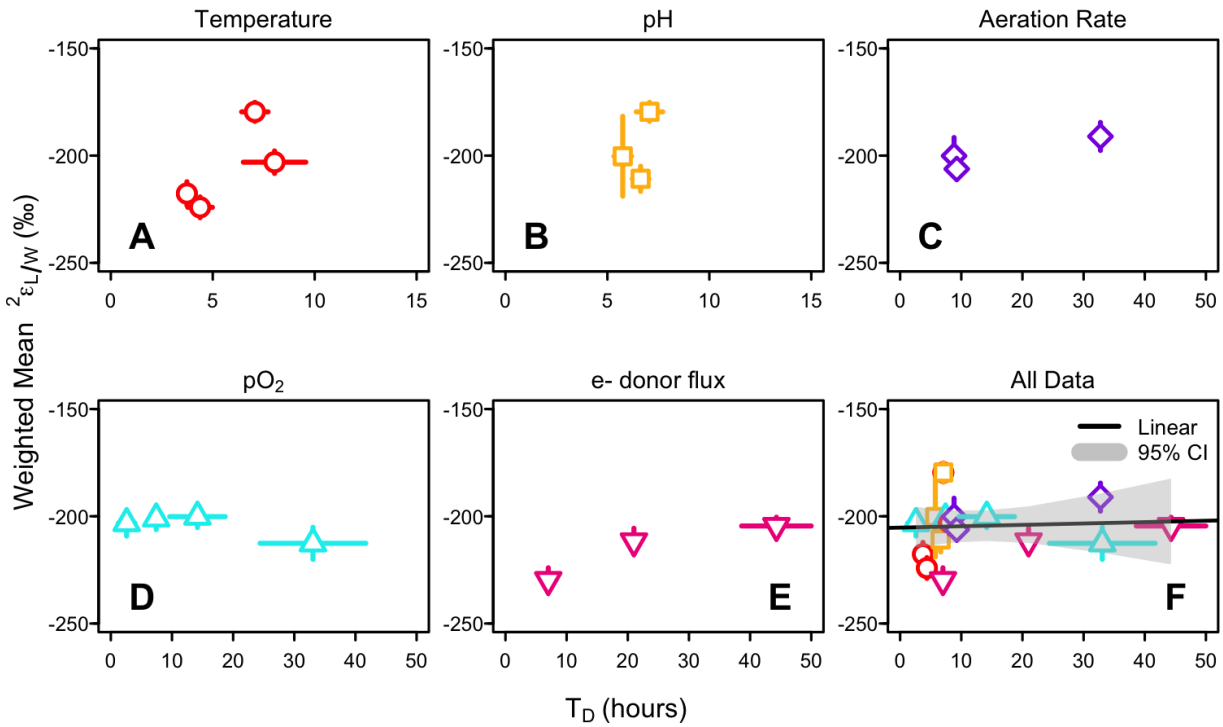

Fig. 5. The abundance weighted H-isotope fractionation ($^{2}\varepsilon_{L/W}$) between growth water and biphytanes (BPs) in response to doubling time (hours) in each individual environmental condition experiment (**A-E**) and pooled across all experiments (**F**). When data from all environmental control experiments is pooled, there is no relationship between doubling time (hours) and abundance weighted mean $^{2}\varepsilon_{L/W}$. Points represent mean of biological and technical replicates for each treatment level. Error bars represent propagated error associated with BP abundance measurements, BP-δ^{2}H measurements, and weighted mean $^{2}\varepsilon_{L/W}$ calculations; bars are smaller than the symbols in many cases.

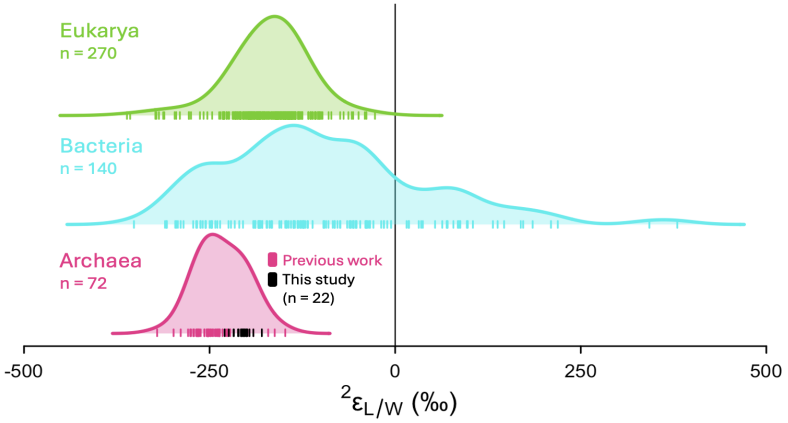

Fig. 6. Summary of lipid/water fractionation ($^{2}\varepsilon_{L/W}$) in culture studies across three domains of life: eukaryotic phototrophs (green; n = 270), bacteria (blue; n = 140), and archaea (pink; n = 72). Tick marks indicate individual $^{2}\varepsilon_{L/W}$ values; shaded curves indicate probability density functions. Archaea data includes measurements of phytanes and biphytanes from *Sulfolobus* sp. (Kaneko et al., 2011), *M. barkeri* (Wu et al., 2020), *N. maritimus* (Leavitt et al., 2022), *Acidianus* sp. DS80, *A. fulgidus*, and *Metallosphaera sedula* (Rhim et al., 2024), and *S. acidocaldarius* (this study; black tick marks). Data for Eukarya and Bacteria is redrawn from Rhim et al., (2024), Figure 6. Eukarya data includes measurements for acetogenic and isoprenoid lipids. Bacteria data includes fatty acids synthesized by multiple metabolisms (e.g., aerobic and anaerobic heterotrophy, aerobic and anaerobic chemoautotrophy, and photoautotrophy).